Original Investigation

Comparison of Hyperpolarized ^{3}He and ^{129}Xe MR Imaging in Cystic Fibrosis Patients

Ummul Afia Shammi, MS, Michelle Felicia D'Alessandro, BS, Talissa Altes, MD, F. William Hersman, PhD, Iulian C. Ruset, PhD, John Mugler III, PhD, Craig Meyer, PhD, Jamie Mata, PhD, Kun Qing, PhD, Robert Thomen, PhD

Purpose: In this study, we compared hyperpolarized ^{3}He and ^{129}Xe images from patients with cystic fibrosis using two commonly applied magnetic resonance sequences, standard gradient echo (GRE) and balanced steady-state free precession (TrueFISP) to quantify regional similarities and differences in signal distribution and defect analysis.

Materials and Methods: Ten patients (7M/3F) with cystic fibrosis underwent hyperpolarized gas MR imaging with both ^{3}He and ^{129}Xe. Six had MRI with both GRE, and TrueFISP sequences and four patients had only GRE sequence but not TrueFISP. Ventilation defect percentages (VDPs) were calculated as lung voxels with $<$60% of the whole-lung hyperpolarized gas signal mean and was measured in all datasets. The voxel signal distributions of both ^{129}Xe and ^{3}He gases were visualized and compared using violin plots. VDPs of hyperpolarized 3 He and 129 Xe were compared in Bland-Altman plots; Pearson correlation coefficients were used to evaluate the relationships between inter-gas and inter-scan to assess the reproducibility.

Results: A significant correlation was demonstrated between ^{129}Xe VDP and ^{3}He VDP for both GRE and TrueFISP sequences ($\rho = 0.78$, $p < 0.0004$). The correlation between the GRE and TrueFISP VDP for ^{3}He was $\rho = 0.98$ and was $\rho = 0.91$ for ^{129}Xe. Overall, ^{129}Xe (27.2$\pm$9.4) VDP was higher than ^{3}He (24.3$\pm$6.9) VDP on average on cystic fibrosis patients.

Conclusion: In patients with cystic fibrosis, the selection of hyperpolarized ^{129}Xe or ^{3}He gas is most likely inconsequential when it comes to measure the overall lung function by VDP although ^{129}Xe may be more sensitive to starker lung defects, particularly when using a TrueFISP sequence.

KEY WORDS: Hyperpolarized MRI; Ventilation defect percentage; Cystic fibrosis; Lung defects; MRI scan.

Abbreviations: ADC Apparent Diffusion Coefficient, **ANOVA** Analysis of Variance, **CF** Cystic Fibrosis, **CFTR** Cystic Fibrosis Transmembrane Conductance Regulator, **COPD** Chronic Obstructive Pulmonary Disease, **GRE** Gradient Echo, **HP** Hyperpolarized, **HPG** Hyperpolarized Gas, **ILD** Interstitial Lung Disease, **IRB** Institutional Review Board, **MRI** Magnetic Resonance Imaging, **NMR** Nuclear Magnetic Resonance, **NSCLC** Nonsmall-Cell Lung Cancer, **SNR** Signal-to-Noise Ratios, **TCV** Thoracic Cavity Volume, **TrueFISP** Fast Imaging with Steady Precession (Balanced Steady State Free Precession), **VDP** Ventilation Defect Percentage, **VV%** Percentage Ventilated Volume

INTRODUCTION

Hyperpolarized (HP) gas magnetic resonance imaging (1) is a noninvasive and nonionizing imaging technique that reveals high-resolution information related to lung function and microstructure. While initial HP gas studies were performed with ^{129}Xe (2) focus quickly shifted to ^{3}He because of its higher gyromagnetic ratio and greater achievable polarization and thus higher NMR signal. Helium-3 (^{3}He) MRI has demonstrated impressive sensitivity to regional lung function in myriad lung diseases such as cystic fibrosis (3,4) asthma (5–7) chronic obstructive pulmonary disease (COPD) (8) and others and has elucidated new information related to lung function (9–13), disease severity and

Acad Radiol 2021; ■:1–9

From the Biomedical, Biological, and Chemical Engineering, University of Missouri, Columbia, Missouri (U.A.S., R.T.); School of Medicine, University of Missouri, Columbia, Missouri (M.F.D.); Radiology, School of Medicine, University of Missouri, Columbia, Missouri (T.A., R.T.); Physics, University of New Hampshire, Durham, New Hampshire (F.W.H.); Xemed, LLC, Durham, New Hampshire (I.C.R.); Radiology and Medical Imaging, University of Virginia School of Medicine, Charlottesville, Virginia (J.M., C.M., J.M., K.Q.); Biomedical Engineering, University of Virginia, Charlottesville, Virginia (J.M., C.M.). Received September 10, 2020; revised December 24, 2020; accepted January 6, 2021. Funded by Vertex Pharmaceuticals. **Address correspondence to:** R.T. e-mail: thomenr@health.missouri.edu

https://doi.org/10.1016/j.acra.2021.01.007

progression (14-17), parenchymal microstructure (18,19) and translational efficacy (20). However, its terrestrial scarcity and high price have made it undesirable for routine clinical use in recent years (21). As hyperpolarization methods and technology have continued to develop, achievable ^{129}Xe polarizations, MRI image quality, and SNR have substantially improved and made ^{129}Xe MRI a comparable alternative to ^{3}He. Researchers in this field are now motivated to shift towards the use of cheaper and naturally available ^{129}Xe as translational studies, and clinical trials are underway (22-27). Head-to-head comparisons of ^{3}He and ^{129}Xe images in COPD and asthma have revealed similar intra-subject ventilation patterns indicating that the two gases are largely interchangeable in these diseases (28-30). However, to our knowledge, similar studies in cystic fibrosis lung disease have not been previously published. Because CF lung disease exhibits myriad pathological abnormalities (e.g., bronchiectasis, mucus plugs, consolidations), the ventilation patterns of ^{129}Xe/^{3}He may demonstrate greater discrepancies (31). Here we have quantitatively and regionally compared ^{3}He and ^{129}Xe MR images in subjects with CF lung disease in order to examine similarities and differences in ventilation patterns between the two gases.

Previous studies have compared pulmonary ventilation and diffusion MR images with HP ^{3}He and ^{129}Xe in COPD, asthma, emphysema, nonsmall-cell lung cancer (NSCLC) and in healthy subjects (28-30). The results showed significant statistical correlation between the whole lung ventilation defect percentage (VDP), apparent diffusion coefficient (ADC), and percentage ventilated volume (VV%). However, the VDP was significantly greater for ^{129}Xe imaging than that with ^{3}He for patients with COPD, and likewise, the ventilated volume percentages (VV%) was higher for ^{3}He in COPD and NSCLC patients. This is likely due to much lower diffusivity of ^{129}Xe compared with ^{3}He (D_{129Xe}=0.12 cm^2/s vs D_{3He}=0.88 cm^2/s dilute in air), resulting in slower penetration into partially obstructed airways. Nevertheless, these studies concluded that both gases provided comparable information of lung microstructure and ventilation in these diseases. HP ^{3}He and ^{129}Xe MRI have also demonstrated sensitivity to cystic fibrosis lung function impairment, which occurs due to a mutation in cystic fibrosis transmembrane conductance regulator (CFTR) and results in bronchial wall thickening, mucus plugging, tissue destruction, bronchiectasis, and airspace consolidation (3,16,20,25,32-38). Furthermore, same and multiday imaging along with interscan repeatability has been tested with HP ^{3}He and ^{129}Xe in CF, showing consistent images over 20 minutes (38) and over a span of 4 weeks period time (39). In a recent study, ventilation defects seen in ^{129}Xe images of CF patients were regionally associated with corresponding structural abnormalities seen on UTE MRI, and it was found that 49% of the ^{129}Xe defect volume across all subjects could not be attributed to an apparent structural abnormality – a finding that highlights the sensitivity of ^{129}Xe MRI to ventilatory impairment (40).

In this study, we have performed a direct quantitative analysis of ^{3}He and ^{129}Xe ventilation imaging in CF subjects using two of the most commonly employed MR sequences: the standard gradient echo (GRE) and balanced steady-state free precession (TrueFISP). The TrueFISP sequence is known to yield greater NMR signal per unit time, a desirable trait for imaging HP gases (41), but the signal intensity distributions between TrueFISP and GRE images may not necessarily be congruent within the same patient; thus we chose to simultaneously evaluate ventilation differences inter-gas and inter-sequence to investigate the repeatability and compatibility of these protocols. This evaluation is important as imaging centers begin multisite studies involving ^{129}Xe MRI as a biomarker in upcoming clinical trials (42).

MATERIALS AND METHODS

The study was approved from the institutional review board (IRB), and written informed consent was obtained from all subjects. Seven male and three female subjects diagnosed with cystic fibrosis and with no smoking history were recruited (mean age 33 ± 7 years, range 23-50). Patient demographic data are given in Table 1. All subjects went through spirometry according to American Thoracic Society guidelines (43) (Koko Spirometer; nSpire, Longmont, Colorado) and peripheral capillary oxygen saturation (SpO_2) before and after each MRI scan.

TABLE 1. Demographic Description of the CF Subjects

Subject	Age [year]	Gender	Height [inches]	Weights [lb]	BMI	FEV_1 [% predicted]	FVC [L]
1	44	M	64	132	22	39	1.73
2	28	M	68	147	22	58	4.23
3	31	M	65	138	23	82	4.91
4	24	F	67	130	20	71	3.44
5	33	M	65	140	23	88	5.01
6	26	M	67	157	24	77	4.21
7	23	M	73	149	20	61	4.9
8	32	F	64	128	22	94	3.52
9	36	M	72	185	25	88	5.9
10	50	F	67	138	21	98	4.22

FEV1- Forced expiratory volume in 1 second, FVC- Forced vital capacity.

MR Image Acquisition

MR images were acquired on a 1.5T Siemens Avanto (Siemens Medical Solutions). ^{3}He gas was polarized via spin-exchange optical-pumping using either a prototype commercial system (Model 9600, Magnetic Imaging Technologies Inc., Durham North Carolina) or a custom-built system (44) to obtain polarization levels of 35 or 60%, respectively. ^{129}Xe was polarized by using a XeBox-E10 (Xemed, LLC, Durham, North Hampshire) to polarization of 40%. He MR imaging was performed in a Tx/Rx rigid chest radio-frequency (RF) coil (Rapid Biomedical, Rimpar, Germany). This RF coil was equipped with proton-blocking circuits to allow ^{1}H imaging of the chest using the body RF coil of the MR scanner with the He^{3} RF coil in place. A flexible, Tx/Rx circularly-polarized, vest-shaped chest RF coil (Clinical MR Solutions, Brookfield, WI) was used for all HP ^{129}Xe MRI acquisitions. All the breath-hold images were collected within 15 seconds for all subjects. Prior to imaging, each subject underwent a short flip-angle calibration sequence with a small amount of HP gas. Six of the ten patients had MRI with both gradient echo (GRE) and steady-state free precession (TrueFISP) sequences and four patients had only GRE sequence but not TrueFISP due to technical issues. Depending on the lung size for each subject, around 13-17 contiguous coronal slices with a slice thickness of 15 mm were acquired to cover the whole lung. Imaging parameters for both ^{3}He and ^{129}Xe GRE were: acquisition matrix: 96 × 90, flip angle = 10°, slice thickness = 15 mm, TR= 6.05-9.4, TE = 2.3-3.7ms, field of view = 360 × 384. Imaging parameters for both the gases in TrueFISP were acquisition matrix: 96 × 90, flip angle = 25-40°, slice thickness = 15 mm, TR= 2.57-4.5, TE = 1.1-2ms, field of view = 360 × 384.

All subjects were trained to inhale room air and breath-hold for 12-15 seconds before doing the MR imaging. HP gas was dispensed into a Tedlar bag (Jensen Inert Products, Coral Springs, Florida) and diluted with medical-grade nitrogen or oxygen to a total volume equaling approximately one-third of the subject's forced vital capacity as determined from spirometry. Inhaled volumes for ^{3}He and ^{129}Xe were within 200mL of each other to ensure consistent lung inflation levels within the same subject (^{3}He and ^{129}Xe dosages are given for each patient in Table 2) with the exception of subject 3 whose total inhaled gas volume was 1400ml for ^{3}He imaging and 850ml for ^{129}Xe imaging. ^{129}Xe gas mixtures (nitrogen/oxygen balance) varied throughout the study due to IRB modification and/or alterations (dosage data for subject 2 was lost). Each subject began dose inhalation from residual volume (RV), and continuous physiologic monitoring was conducted by a nurse during the image acquisitions. The order of ^{3}He and ^{129}Xe MR acquisitions were randomized for each patient. In between each gas image acquisition, the subject was brought out of the scanner, the multinuclear coils were swapped, and the subject was quickly re-localized for the next acquisition. For subjects imaged with both GRE and TrueFISP, the GRE was always acquired first.

Image Analysis

Signal to Noise Ratios (SNR) were calculated for each acquired image set as the mean signal within the whole-lung boundary divided by the standard deviation of the noise floor (manually-selected region outside the lung). RF correction was performed using N3 ITK bias correction onto both sets of images as difference in the ^{3}He and ^{129}Xe receiver coil shows RF sensitivity profile (45). Manual segmentation of the lung from ^{3}He and ^{129}Xe breath-hold images was performed separately for each acquisition using 3D slicer image analysis software (46), and descriptive analyses of the images were performed using R statistical computing platform. Each subject's ^{129}Xe images were registered to corresponding ^{3}He images using custom software in Matlab (MathWorks, Natick, Massachusetts) for voxel-wise signal comparisons. Defects were identified in each ventilation image set by calculating the percentage of all lung voxels with <60% of the mean whole-lung HP gas signal and subsequently applying a median filter (3 × 3 kernel) to the resultant binary defect map

TABLE 2A. Dosing Volumes for ^{3}He Images. All values given in milliliters [mL]. Subjects 5, 7, 8, and 10 were not imaged by TrueFISP

	Dose for GRE			Dose for TrueFISP		
Subject No.	^{3}He	N_2 gas	Total Volume	^{3}He	N_2 Gas	Total Volume
1	300	200	500	300	200	500
2	500	570	1070	500	570	1070
3	540	860	1400	540	860	1400
4	500	480	980	500	480	980
5	500	1100	1600	-	-	-
6	540	660	1200	540	660	1200
7	500	1180	1680	-	-	-
8	300	700	1000	-	-	-
9	600	1120	1720	400	1320	1720
10	500	1000	1500	-	-	-

TABLE 2B. Dosing volumes for ^{129}Xe images. All values given in milliliters [mL]. Subjects 5, 7, 8, and 10 were not imaged by TrueFISP. Dosing information for subject 2 could not be found

	Dose for GRE				Dose for TrueFISP			
Subject No.	^{129}Xe	O_2 Gas	N_2 Gas	Total Volume	^{129}Xe	O_2 Gas	N_2 Gas	Total Volume
1	500	-	-	500	500			500
2	*	*	*	*	*	*	*	*
3	600	250	-	850	600	250	-	850
4	700	230	-	930	600	230	-	830
5	1000	-	600	1600	-	-	-	-
6	800	500	-	1300	800	500		1300
7	1000	-	600	1600	-	-	-	-
8	1000	-	200	1200	-	-	-	-
9	850	250	750	1850	850	250	750	1850
10	1000	-	500	1500	-	-	-	-

(13,25). The ventilation defect percentage (VDP) was calculated as the percentage of whole-lung volume marked as defect. VDP was calculated for both registered and unregistered ^{129}Xe images to verify consistency following registration. For comparing the regional VDP calculation of both the gases, voxels from the registered ^{129}Xe and ^{3}He images for each subject were divided into four groups: voxels identified as defect in both ^{3}He and ^{129}Xe scans, voxels identified as defect in ^{3}He but not xenon scans and vice versa, and non-defect voxels in both gas images. In order to evaluate a minimum acceptable SNR for VDP calculation, we added Gaussian noise of increasing standard deviation to the real and imaginary channels of the k-space data of one image set before Fourier transformation and subsequent VDP calculation.

Statistical Analysis

SNR was compared between gases and between MRI scan types using means and standard deviations for all subjects, and a Pearson correlation coefficient between dataset SNR and VDP was calculated. Violin plots were created to illustrate ^{129}Xe and ^{3}He voxel signal distributions for visual comparison of signal distributions between the two gases. Pearson correlation coefficients and Bland-Altman plots were created between ^{3}He and ^{129}Xe VDP's for all scans as well as separately for GRE and TrueFISP scans. A Pearson correlation coefficient was used to compare VDP's between GRE and TrueFISP scans for each gas separately. Voxel wise comparison between ^{3}He and ^{129}Xe images were assessed for each patient using Pearson correlation coefficients. P values less than 0.05 were considered significant. The effect of the scanning order on VDP measurement was tested by calculating repeated measures ANOVA.

RESULTS

HP gas imaging procedures were well tolerated by all subjects, and no serious or severe adverse events were reported. There was a single respiratory adverse event reported by one patient (subject 10) who had tightness in throat and voice dropped after inhalation. Subject demographic data and spirometric results are shown in Table 1. All of the subjects were Caucasian, non-smokers.

Mean SNR for ^{3}He and ^{129}Xe GRE sequences was 141±45 and 67±30 respectively, and TrueFISP sequence was 217±80 and 116.5±21 respectively. The SNR information, along with subject VDP, are reported in Table 3 for each subject. Adding simulated noise to the real and imaginary channels of ^{3}He and ^{129}Xe k-space data revealed that the VDP calculation is robust for SNR greater than approximately 10 in the reconstructed images (Fig 1). Further, there was no correlation between VDP and SNR measurement (ρ = -0.119, p-value = 0.515).

No significant correlation was found between the difference in measured VDP and difference in inhaled gas volume calculated as a percentage of FVC (ρ=0.54, p= 0.1306 for GRE and ρ=0.0.0687, p= 0.9126 for TrueFISP), however, the largest difference in VDP was measured in subject 3 whose inhaled gas volumes differed by 550 mL (mean VDP_{3He} = 24.5%, VDP_{129Xe} = 34.6%, Vol_{3He} = 1400 ml, Vol_{129Xe} = 850 ml). Individual subject VDP's were higher on average in ^{129}Xe images vs ^{3}He images (mean ΔVDP = mean ($VDP_{129Xe} - VDP_{3He}$) = 4.7 ± 3.21).

Figure 2 shows example ^{3}He and ^{129}Xe GRE images and defect analysis from two representative subjects. Subject 6 (top set of images) has excellent concordance between the ^{3}He and ^{129}Xe ventilation defects; whereas, Subject 3 (bottom set of images) has more and larger ventilation defects with ^{129}Xe (the difference in subject 3's inhaled gas volume between ^{3}He and ^{129}Xe images was 550 mL). The ^{3}He and ^{129}Xe VDP for each subject is given in Table 3. In 6 of 10 (60%) subjects, the ^{3}He and ^{129}Xe GRE VDP were within 5 points, but 4 of 10 (40%) subjects had a larger variation between the ^{3}He and ^{129}Xe GRE VDP. In 9 of the 10 subjects, the ^{129}Xe GRE VDP was equal to or larger than the ^{3}He GRE VDP. Figure 3 shows central coronal slices of ^{3}He and ^{129}Xe MR images in both GRE and TrueFISP scans for all subjects in order vertically from the highest average VDP to lowest. The appearance of and the VDP calculated from

TABLE 3. VDP and SNR of all Subjects

Subject No	First scan gas	VDP [%] ^{3}He GRE	SNR ^{3}He GRE	VDP [%] ^{3}He TF	SNR ^{3}He TF	Mean ^{3}He VDP [%]	VDP [%] ^{129}Xe GRE	SNR ^{129}Xe GRE	VDP [%] ^{129}Xe TF	SNR ^{129}Xe TF	Mean ^{129}Xe VDP [%]
1	^{129}Xe	37.0	54.2	33.2	133	35.1	40.0	34.6	47.3	95.7	43.65
2	^{3}He	35.1	172.6	32.3	268.8	33.7	28.0	48.5	29.0	105.4	28.5
3	^{129}Xe	25.0	118	24.0	139.9	24.5	35.6	80.4	33.6	158	34.6
4	^{3}He	26.6	202.9	26.7	304.1	26.65	27.1	73.3	33.8	118.8	30.45
5	^{129}Xe	20.6	148.4	-	-	20.6	25.3	34.2	-	-	25.3
6	^{3}He	21.2	130.6	21.0	296	21.1	24.4	60.2	24.3	106.9	24.35
7	^{3}He	19.0	170.5	-	-	19	26.5	74.1	-	-	26.5
8	^{129}Xe	16.9	81.5	-	-	16.9	16.8	138.7	-	-	16.8
9	^{3}He	18.4	162.2	16.7	160.2	17.55	14.7	48.3	15.0	114.3	14.85
10	^{3}He	15.4	169.4	-	-	15.4	14.3	77.4	-	-	14.3

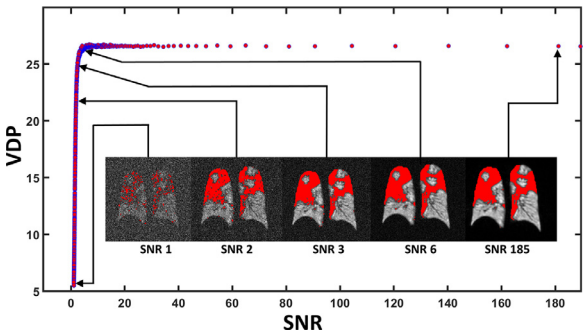

Figure 1. Plot of calculated VDP as a function of SNR and representative slices for subject 4. Gaussian noise of increasing standard deviation was added to the k-Space data of this image set before Fourier Transform and VDP calculation. VDP is consistent for SNR values above approximately 10.

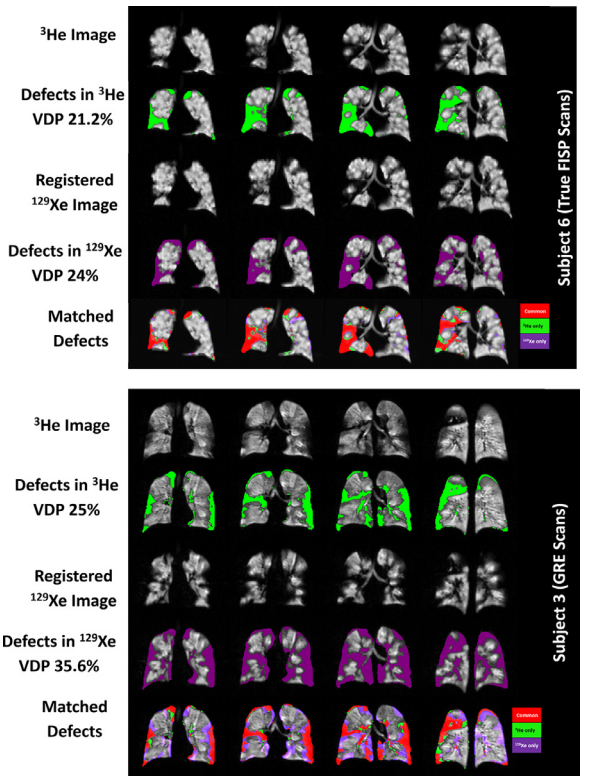

Figure 2. Example images illustrating defect analysis for both ^{3}He and registered ^{129}Xe gas images. Subject 6 has excellent concordance between the ^{3}He and ^{129}Xe ventilation defects, whereas, Subject 3 has more and larger ventilation defects with ^{129}Xe.

the GRE and TrueFISP images demonstrate similar patterns of ventilation distribution and signal intensity, though not identical. Violin plots of ^{3}He and ^{129}Xe signal distribution in GRE and TrueFISP are shown in Figure 4. Plots are normalized to the signal distribution's 95th percentile voxel signal value, and the red lines indicate the calculated defect threshold for each image set (60% of the mean). Of note, the signal intensity distribution for ^{3}He and ^{129}Xe GRE is very similar in some subjects (e.g., Subjects 4, 6, 8, and 10); while in other subjects, the ^{129}Xe signal intensity distribution is skewed toward lower intensity values (e.g., Subjects 3 and 7). Subject 2 was the only subject with the signal intensity distribution skewed lower for ^{3}He. As shown in Figure 3, Subject 2 had better ventilation of abnormal regions in the bilateral upper lobes with ^{129}Xe than ^{3}He.

To evaluate the regional signal correspondence between the gases, ^{129}Xe images were registered to ^{3}He images in each subject, and Pearson correlation coefficients were calculated between original ^{129}Xe and registered ^{129}Xe voxel signals for all voxels within the boundary of the lung parenchyma (average $\rho = 0.94 \pm 0.25$). Figure 5 presents a color-coded bar plot showing each subject's percentage of lung volume identified as defective or normal for each gas. This regional analysis shows that the fraction of lung volume with congruent classification between ^{3}He and ^{129}Xe GRE (gray plus red bars) ranged from 82 to 95%. The areas of discordance between ^{3}He and ^{129}Xe GRE defects had a greater defective volume for ^{129}Xe than ^{3}He in 8 of the 10 subjects. Bland-Altman plot of the VDPs in Figure 6b shows that ^{129}Xe VDP was higher compared to ^{3}He in most of the cases (overall mean of the VDP differences was -2.9). Although the VDP is higher for ^{129}Xe, the scatter plot (Fig 6a) shows the similar trends between the VDPs of the two gas distributions in all

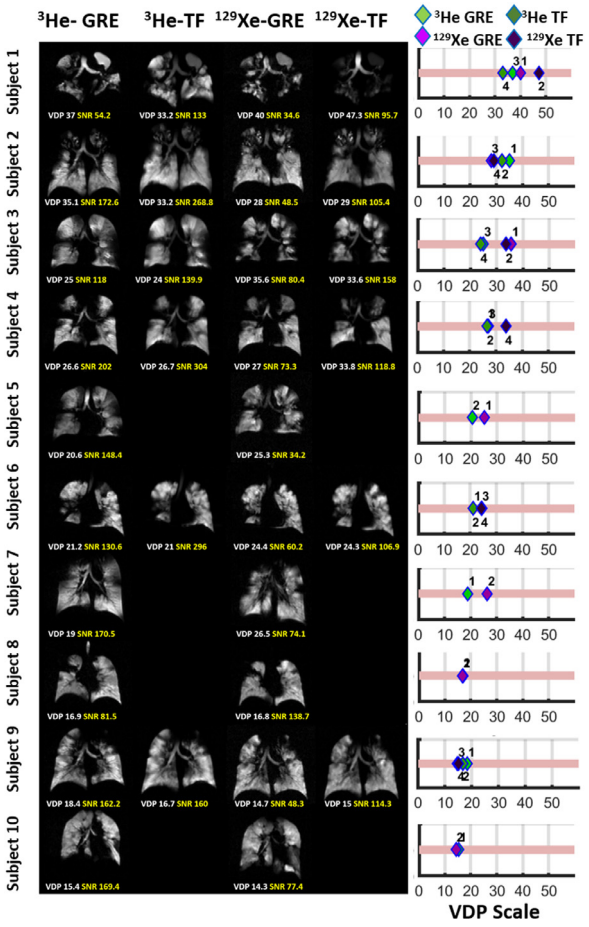

Figure 3. Representative slices of ^{3}He and ^{129}Xe MR images for all subjects alongside whole-lung VDP measures for each scan. The numbers in the VDP scale represents the scan order.

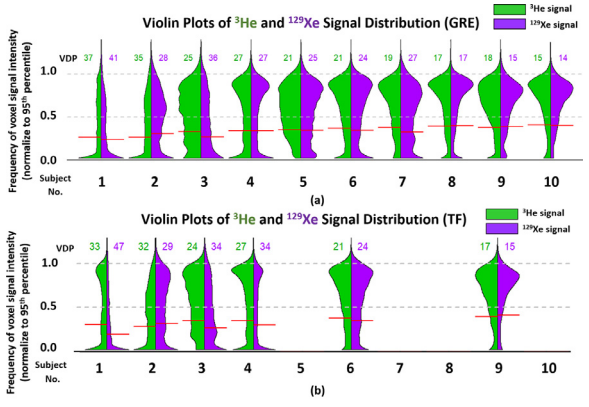

Figure 4. Violin plot of whole-lung ^{3}He vs ^{129}Xe voxel signal intensity distributions for each subject's (a) GRE and (b) TrueFISP data. All datasets are normalized 95th percentile voxel signal value, and defect threshold values (60% of the whole-lung signal mean) are given for each dataset by the horizontal red lines. Each dataset's calculated VDP is given above each violin plot.

subjects (^{3}He/^{129}Xe VDP correlation coefficient between all scans $\rho = 0.78$, slope= 1.02, $p = 0.00036$). The correlation between the GRE and TrueFISP VDP for ^{3}He was ρ=0.98 and was ρ=0.91 for ^{129}Xe. The entire cohort had a Pearson correlation coefficient of $\rho = 0.75$ between ^{3}He and ^{129}Xe voxel signal ($p < 2.2 \times 10^{-16}$). The result of repeated measures ANOVA indicates that the VDP was independent of scanning order (F = 0.265).

DISCUSSION

We compared ^{3}He and ^{129}Xe MR images in subjects with CF and found that (1) VDP obtained with ^{129}Xe (27.2±9.4) was higher on average compared to ^{3}He (24.3±6.9) (mean ΔVDP = mean ($VDP_{129Xe} - VDP_{3He}$) = 4.7 ± 3.21), (2) ^{3}He and ^{129}Xe reveal comparable maps of ventilation by voxel-wise signal correlations ($\rho = 0.75$, $p < 2.2 \times 10^{-16}$), (3) differences in total inhaled gas volumes may lead to inconsistencies in measured VDPs which do not reflect underlying physiology. A significant correlation between ^{3}He and ^{129}Xe VDP was found for both GRE and TrueFISP sequences ($\rho = 0.78$, p<0.0004). Defects exhibited in ^{129}Xe images demonstrated more pronounced boundaries compared with ^{3}He and may be a consequence of the differing gas diffusivities. Figure 2 highlights this difference between a case with a small VPD difference and a case with a large VDP difference.

The result of this study also corroborates conclusions of previous studies that were done with HP ^{3}He and ^{129}Xe on lung patients. Kirby et al. demonstrated a significant correlation between whole lung ^{3}He and ^{129}Xe VDP (r=0.91, p <0.0001) for patients with COPD, although VDP was higher for ^{129}Xe images than for ^{3}He (9% ± 8 bias) (29). Stewart et al. also observed a positive correlation between ^{3}He and ^{129}Xe VV (r = 0.86, p <0.001) on COPD and NSCLC patients, and here also, VV% was larger for ^{3}He than for ^{129}Xe (average bias 8.79%) (30). This shows that the conclusion of both these studies is consistent with ours.

The slope of ^{129}Xe VDP vs. ^{3}He VDP was steeper for True FISP scans ($y = 1.18x + 0.94$) compared with GRE ($y = 0.90x + 4.18$), indicating that TrueFISP scans may depict more defects on ^{129}Xe images compared with ^{3}He than on GRE scans (Fig 6a).

SNR of TrueFISP images was overall higher than GRE for both gases as expected. SNR in all image sets was more than adequate to ensure accurate VDP calculation (lowest SNR of 34.6 in subject 1). In our method, we have chosen to identify defects as voxels with signal less than 60% of the whole-lung signal mean and median-filtering the resultant binary defect map, but other groups have had success using more stratified analysis approaches including k-means delineation (29) and normalization to the 99th percentile signal value (47). However, the 60% method neither requires healthy subject data for voxel binning (48) nor does it require ^{1}H MRI derived thoracic cavity volume (TCV) (15).

We acknowledged that our study is limited by a small number of patients, and there were no healthy subjects in the study for comparison. Therefore, judicious measures need to be taken before reducing these results to the general CF population. We also recognize potential imprecision in the manual segmentation of both ^{3}He and ^{129}Xe images as proton

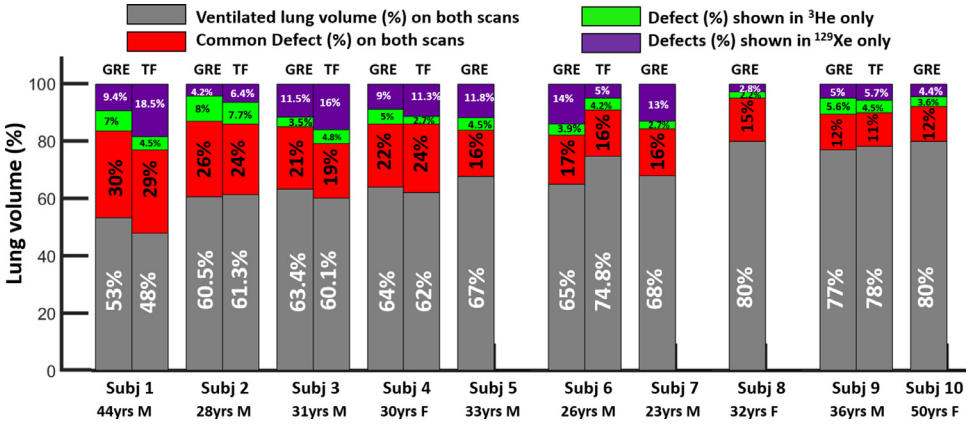

Figure 5. Bar plot showing percentages of classification of voxels in ^{3}He scans and corresponding registered ^{129}Xe scans.

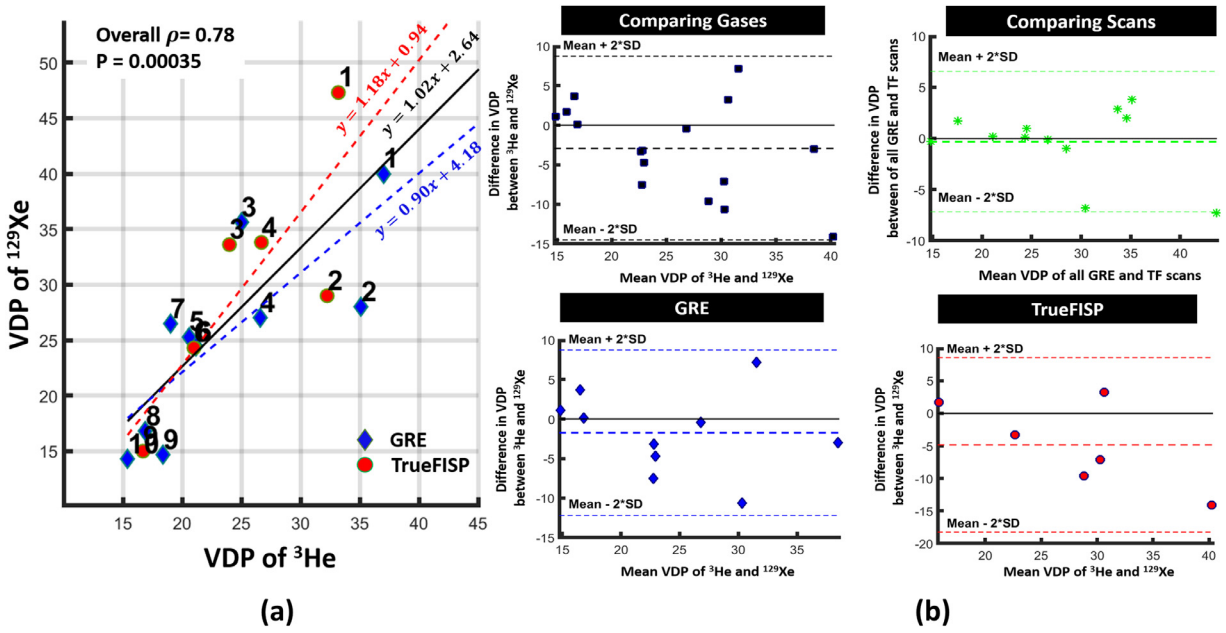

Figure 6. (a) Plot of ^{129}Xe VDP vs ^{3}He VDP showing linear fitted curves for GRE data (blue, $\rho = 0.79$, slope m=0.90), TrueFISP data (red $\rho = 0.81$, slope m= 1.18), and all data (black, $\rho = 0.788$, slope m= 1.02) (b) Bland-Altman plot shows absolute percentage differences between VDP of ^{3}He and ^{129}Xe, VDP in GRE and TrueFISP scans (top panel); GRE only and TrueFISP only (bottom panel). SD, standard deviation. (Color version of figure is available online.)

images were not acquired in the same breath hold. Furthermore, image registration on ^{129}Xe images to compare the common defective region in both gases might not be precise. However, the outcomes were visually inspected by the experts and we do not expect these to affect our results substantially. During the data collection phase of this study, the dosing methodology for ^{129}Xe changed with IRB limitations/modifications. Thus, subjects generally did not receive equivalent volumes of ^{3}He and ^{129}Xe gas in this study. This may be a confounding factor as differences in lung inflation volumes, and disease severity are known to affect HP gas parenchymal distributions and defect percentages. In spite of this discrepancy, the relative congruence in HPG data between the two gases is nonetheless encouraging.

Importantly, total inhaled gas volume likely impacts VDP measurement in addition to underlying lung physiology; thus, consistent dosing strategies must be employed to minimize potential error in VDP due to lung inflation. In our study, while in most of the cases, the total volume administered with ^{3}He and ^{129}Xe were within 200mL of each other (and thus, we did not see a significant correlation between differences VDP and differences in inflation volume), the dosing for subject 3 was inconsistent between imaging sessions and measured VDP difference was large (difference in total volume of gas was 550 ml and the difference in VDP was 10%, Table 3). Because defect regions do not inflate, VDP is expected to decrease as more inhaled gas fills other regions of the lung. We expect this is the primary source of

the VDP difference observed in subject 3, though the trend of ^{3}He images to demonstrate lower VDP than ^{129}Xe images is likely also responsible to an extent. The choice of gas for dilution (nitrogen or oxygen) are considered to be less significant on the resultant images than total inhaled volume which was studied previously by Hughes et al. (2019) (49). Consistent dosing strategies are often employed to obviate this issue, and our choice of 1/3FVC as the inhaled dose volume for most subjects was chosen to ensure HP images were acquired within normal physiologic range. Future work may benefit from examining absolute defect volumes as well as VDP. However, it is critical in future HP gas studies to standardize inflation volume across subjects and ideally across sites, particularly when performing longitudinal follow-ups within the same patient.

In summary, we evaluated the lung ventilation with HP ^{3}He and ^{129}Xe gases onto CF patients with GRE and TrueFISP scans. The VDP was similar to or higher for ^{129}Xe scans relative to ^{3}He in 9 of 10 subjects, which is similar to results from previous studies in other lung diseases. Overall, we find that the choice of ^{3}He vs. ^{129}Xe for HP gas studies is largely inconsequential to the measure of overall lung function by VDP, but xenon may be more sensitive to partial obstructions, particularly when using a TrueFISP sequence. This also supports the use of ^{129}Xe as a less costly surrogate for ^{3}He MRI, especially in longitudinal studies on disease progression and quantifying individual lung defects.

ACKNOWLEDGEMENTS

The authors wish to thank Matthew M. Willmering for guidance using the image registration software (Matlab, Natick Massachusetts). Funding for this study was provided by Vertex Pharmaceuticals.

REFERENCES

1. Verbanck S, King GG, Zhou W, et al. The quantitative link of lung clearance index to bronchial segments affected by bronchiectasis. Thorax Jan 2018; 73(1):82–84.
2. Albert MS, Cates GD, Driehuys B, et al. Biological magnetic resonance imaging using laser-polarized 129Xe. Nature Jul 21 1994; 370(6486):199–201.
3. Kirby M, Svenningsen S, Ahmed H, et al. Quantitative evaluation of hyperpolarized helium-3 magnetic resonance imaging of lung function variability in cystic fibrosis. Acad Radiol Aug 2011; 18(8):1006–1013.
4. Koumellis P, van Beek EJ, Woodhouse N, et al. Quantitative analysis of regional airways obstruction using dynamic hyperpolarized 3He MRI-preliminary results in children with cystic fibrosis. J Magn Reson Imaging Sep 2005; 22(3):420–426.
5. Altes TA, Powers PL, Knight-Scott J, et al. Hyperpolarized 3He MR lung ventilation imaging in asthmatics: preliminary findings. J Magn Reson Imaging Mar 2001; 13(3):378–384.
6. de Lange EE, Altes TA, Patrie JT, et al. Evaluation of asthma with hyperpolarized helium-3 MRI: correlation with clinical severity and spirometry. Chest Oct 2006; 130(4):1055–1062.
7. Tzeng YS, Lutchen K, Albert M. The difference in ventilation heterogeneity between asthmatic and healthy subjects quantified using hyperpolarized 3He MRI. J Appl Physiol (1985) Mar 2009; 106(3):813–822.
8. Salerno M, de Lange EE, Altes TA, Truwit JD, Brookeman JR, Mugler 3rd JP. Emphysema: hyperpolarized helium 3 diffusion MR imaging of the lungs compared with spirometric indexes–initial experience. Radiology Jan 2002; 222(1):252–260.
9. de Lange EE, Mugler 3rd JP, Brookeman JR, et al. Lung air spaces: MR imaging evaluation with hyperpolarized 3He gas. Radiology Mar 1999; 210(3):851–857.
10. Fain SB, Gonzalez-Fernandez G, Peterson ET, et al. Evaluation of structure-function relationships in asthma using multidetector CT and hyperpolarized He-3 MRI. Acad Radiol Jun 2008; 15(6):753–762.
11. Kauczor HU, Ebert M, Kreitner KF, et al. Imaging of the lungs using 3He MRI: preliminary clinical experience in 18 patients with and without lung disease. J Magn Reson Imaging May-Jun 1997; 7(3):538–543.
12. Parraga G, Mathew L, Etemad-Rezai R, McCormack DG, Santyr GE. Hyperpolarized 3He magnetic resonance imaging of ventilation defects in healthy elderly volunteers: initial findings at 3.0 Tesla. Acad Radiol Jun 2008; 15(6):776–785.
13. Thomen RP, Sheshadri A, Quirk JD, et al. Regional ventilation changes in severe asthma after bronchial thermoplasty with (3)He MR imaging and CT. Radiology Jan 2015; 274(1):250–259.
14. Kirby M, Mathew L, Heydarian M, Etemad-Rezai R, McCormack DG, Parraga G. Chronic obstructive pulmonary disease: quantification of bronchodilator effects by using hyperpolarized (3)He MR imaging. Radiology Oct 2011; 261(1):283–292.
15. Mathew L, Kirby M, Etemad-Rezai R, Wheatley A, McCormack DG, Parraga G. Hyperpolarized (3)He magnetic resonance imaging: preliminary evaluation of phenotyping potential in chronic obstructive pulmonary disease. Eur J Radiol Jul 2011; 79(1):140–146.
16. Mentore K, Froh DK, de Lange EE, Brookeman JR, Paget-Brown AO, Altes TA. Hyperpolarized HHe 3 MRI of the lung in cystic fibrosis: assessment at baseline and after bronchodilator and airway clearance treatment. Acad Radiol Nov 2005; 12(11):1423–1429.
17. Samee S, Altes T, Powers P, et al. Imaging the lungs in asthmatic patients by using hyperpolarized helium-3 magnetic resonance: assessment of response to methacholine and exercise challenge. J Allergy Clin Immunol Jun 2003; 111(6):1205–1211.
18. Yablonskiy DA, Sukstanskii AL, Woods JC, et al. Quantification of lung microstructure with hyperpolarized 3He diffusion MRI. J Appl Physiol (1985) Oct 2009; 107(4):1258–1265.
19. Wang C, Altes TA, Mugler 3rd JP, et al. Assessment of the lung microstructure in patients with asthma using hyperpolarized 3He diffusion MRI at two time scales: comparison with healthy subjects and patients with COPD. J Magn Reson Imaging Jul 2008; 28(1):80–88.
20. Smith L, Marshall H, Aldag I, et al. Longitudinal Assessment of Children with Mild Cystic Fibrosis Using Hyperpolarized Gas Lung Magnetic Resonance Imaging and Lung Clearance Index. Am J Respir Crit Care Med Feb 1 2018; 197(3):397–400.
21. Roos JE, McAdams HP, Kaushik SS, Driehuys B. Hyperpolarized Gas MR Imaging: Technique and Applications. Magn Reson Imaging Clin N Am May 2015; 23(2):217–229.
22. Kaushik SS, Cleveland ZI, Cofer GP, et al. Diffusion-weighted hyperpolarized 129Xe MRI in healthy volunteers and subjects with chronic obstructive pulmonary disease. Magn Reson Med Apr 2011; 65(4):1154–1165.
23. Mugler 3rd JP, Altes TA. Hyperpolarized 129Xe MRI of the human lung. J Magn Reson Imaging Feb 2013; 37(2):313–331.
24. Qing K, Ruppert K, Jiang Y, et al. Regional mapping of gas uptake by blood and tissue in the human lung using hyperpolarized xenon-129 MRI. J Magn Reson Imaging Feb 2014; 39(2):346–359.
25. Thomen RP, Walkup LL, Roach DJ, Cleveland ZI, Clancy JP, Woods JC. Hyperpolarized (129)Xe for investigation of mild cystic fibrosis lung disease in pediatric patients. J Cyst Fibros Mar 2017; 16(2):275–282.
26. Virgincar RS, Cleveland ZI, Kaushik SS, et al. Quantitative analysis of hyperpolarized 129Xe ventilation imaging in healthy volunteers and subjects with chronic obstructive pulmonary disease. NMR Biomed Apr 2013; 26(4):424–435.
27. Driehuys B, Martinez-Jimenez S, Cleveland ZI, et al. Chronic obstructive pulmonary disease: safety and tolerability of hyperpolarized 129Xe MR imaging in healthy volunteers and patients. Radiology Jan 2012; 262(1):279–289.
28. Kirby M, Svenningsen S, Kanhere N, et al. Pulmonary ventilation visualized using hyperpolarized helium-3 and xenon-129 magnetic resonance imaging: differences in COPD and relationship to emphysema. J Appl Physiol (1985) Mar 15 2013; 114(6):707–715.
29. Kirby M, Svenningsen S, Owrangi A, et al. Hyperpolarized 3He and 129Xe MR imaging in healthy volunteers and patients with chronic obstructive pulmonary disease. Radiology Nov 2012; 265(2):600–610.
30. Stewart NJ, Chan HF, Hughes PJC, et al. Comparison of (3) He and (129) Xe MRI for evaluation of lung microstructure and ventilation at 1.5T. J Magn Reson Imaging Mar 5 2018; 48(3):632–642.

31. Rafeeq MM, Murad HAS. Cystic fibrosis: current therapeutic targets and future approaches. J Transl Med Apr 27 2017; 15(1):84.
32. Couch MJ, Morgado F, Kanhere N, et al. Assessing the feasibility of hyperpolarized (129) Xe multiple-breath washout MRI in pediatric cystic fibrosis. Magn Reson Med July 2020; 84(1):304–311.
33. Santyr G, Kanhere N, Morgado F, Rayment JH, Ratjen F, Couch MJ. Hyperpolarized Gas Magnetic Resonance Imaging of Pediatric Cystic Fibrosis Lung Disease. Acad Radiol Mar 2019; 26(3):344–354.
34. Kanhere N, Couch MJ, Kowalik K, et al. Correlation of Lung Clearance Index with Hyperpolarized (129)Xe Magnetic Resonance Imaging in Pediatric Subjects with Cystic Fibrosis. Am J Respir Crit Care Med Oct 15 2017; 196(8):1073–1075.
35. Altes TA, Johnson M, Fidler M, et al. Use of hyperpolarized helium-3 MRI to assess response to ivacaftor treatment in patients with cystic fibrosis. J Cyst Fibros Mar 2017; 16(2):267–274.
36. Walkup LL, Thomen RP, Akinyi TG, et al. Feasibility, tolerability and safety of pediatric hyperpolarized (129)Xe magnetic resonance imaging in healthy volunteers and children with cystic fibrosis. Pediatr Radiol Nov 2016; 46(12):1651–1662.
37. Sun Y, O'Sullivan BP, Roche JP, et al. Using hyperpolarized 3He MRI to evaluate treatment efficacy in cystic fibrosis patients. J Magn Reson Imaging Nov 2011; 34(5):1206–1211.
38. Woodhouse N, Wild JM, van Beek EJ, Hoggard N, Barker N, Taylor CJ. Assessment of hyperpolarized 3He lung MRI for regional evaluation of interventional therapy: a pilot study in pediatric cystic fibrosis. J Magn Reson Imaging Nov 2009; 30(5):981–988.
39. O'Sullivan B, Couch M, Roche JP, et al. Assessment of repeatability of hyperpolarized gas MR ventilation functional imaging in cystic fibrosis. Acad Radiol Dec 2014; 21(12):1524–1529.
40. Thomen RP, Walkup LL, Roach DJ, et al. Regional Structure-function in Cystic Fibrosis Lung Disease Using Hyperpolarized (129)Xe and Ultrashort Echo Magnetic Resonance Imaging. Am J Respir Crit Care Med Jul 15 2020; 202(2):290–292.
41. Bieri O, Scheffler K. Fundamentals of balanced steady state free precession MRI. J Magn Reson Imaging Jul 2013; 38(1):2–11.
42. Couch MJ, Thomen R, Kanhere N, et al. A two-center analysis of hyperpolarized (129)Xe lung MRI in stable pediatric cystic fibrosis: Potential as a biomarker for multi-site trials. J Cyst Fibros Sep 2019; 18(5):728–733.
43. Miller MR, Hankinson J, Brusasco V, et al. Standardisation of spirometry. Eur Respir J Aug 2005; 26(2):319–338.
44. Komlosi P, Altes TA, Qing K, et al. Signal-to-noise ratio, T2, and T2* for hyperpolarized helium-3 MRI of the human lung at three magnetic field strengths. Magn Reson Med Oct 2017; 78(4):1458–1463.
45. Nicholas J, Tustison JCG. N4ITK: Nick's N3 ITK Implementation For MRI Bias Field Correction. The Insight Journal 2009: 1–8.
46. Fedorov A, Beichel R, Kalpathy-Cramer J, et al. 3D Slicer as an image computing platform for the Quantitative Imaging Network. Magn Reson Imaging Nov 2012; 30(9):1323–1341.
47. He M, Zha W, Tan F, Rankine L, Fain S, Driehuys B. A Comparison of Two Hyperpolarized (129)Xe MRI Ventilation Quantification Pipelines: The Effect of Signal to Noise Ratio. Acad Radiol Jul 2019; 26(7):949–959.
48. He M, Kaushik SS, Robertson SH, et al. Extending semiautomatic ventilation defect analysis for hyperpolarized (129)Xe ventilation MRI. Acad Radiol Dec 2014; 21(12):1530–1541.
49. Hughes PJC, Smith L, Chan HF, et al. Assessment of the influence of lung inflation state on the quantitative parameters derived from hyperpolarized gas lung ventilation MRI in healthy volunteers. J Appl Physiol (1985) Jan 1 2019; 126(1):183–192.